Journal of Power Sources 354 (2017) 85–91

Contents lists available at ScienceDirect

Journal of Power Sources

journal homepage: www.elsevier.com/locate/jpowsour

Hierarchical carbon cloth supported $Li_4Ti_5O_{12}$@$NiCo_2O_4$ branched nanowire arrays as novel anode for flexible lithium-ion batteries

Fenghua Xu [a], Fangli Yu [b], Chao Liu [a], Pengde Han [a], Baicheng Weng [a, *]

[a] School of Materials Engineering, Yancheng Institute of Technology, 211 East Jianjun Road, Yancheng, Jiangsu Province, 224051, China
[b] School of Materials Engineering, Xi'an Aeronautical University, 9 Lantian Shi Road, Xi'an, Shaanxi province, 710089, China

HIGHLIGHTS

- $Li_4Ti_5O_{12}$@$NiCo_2O_4$ branching nanowires grown on the surface of carbon cloth.
- Capacity and rate performance of $Li_4Ti_5O_{12}$ based composited is enhanced.
- The flexibility and zero volume changes maintained due to branching NW structure.

ARTICLE INFO

Article history:
Received 25 November 2016
Received in revised form
25 March 2017
Accepted 8 April 2017
Available online 14 April 2017

Keywords:
Carbon cloth
$Li_4Ti_5O_{12}$
$NiCo_2O_4$
Hierarchical structure
Lithium-ion batteries

ABSTRACT

The hierarchical carbon cloth supported $Li_4Ti_5O_{12}$@$NiCo_2O_4$ branched nanowire (NW) arrays were fabricated as the flexible, binder-free anode for lithium-ion batteries. The novel composite exhibits greatly improved specific capacity and rate capability as well as excellent cyclic stability compared to carbon cloth supported $Li_4Ti_5O_{12}$ NW arrays. The results clearly demonstrate that branched growth of $NiCo_2O_4$ NWs on the surface of $Li_4Ti_5O_{12}$ NWs on carbon cloth enhances lithium diffusion. The superior electrochemical performance is ascribed to the unique architecture as well as the synergetic effect of good flexibility and high conductivity of carbon cloth, almost zero volume change during charge/discharge process of $Li_4Ti_5O_{12}$, and high capacity and conductivity of $NiCo_2O_4$. This novel anode possesses high potential for applications in high-performance, flexible lithium-ion batteries.

1. Introduction

The design of high-performance electronic/electric systems including portable electronic devices and hybrid electric vehicles demands robust energy-storage devices with high volumetric/gravimetric energy density as well as environmental benignity [1–6]. Currently, rechargeable lithium-ion batteries (LIBs) are the predominant power source for portable/small electronics [7]. However, the power density and safety should be further improved to meet the requirements of ever-growing development of electronic/electric devices [8]. For instance, graphite is a widely used anode material in commercial LIBs, but it suffers from a safety issue that arises from the formation of dendritic lithium due to the low Li insertion into carbonous materials [9]. Numerous efforts have been made to address these issues through developing high-performance electrode materials [8–22]. In particular, many attentions have been put on transitional metal oxides [8–20].

$Li_4Ti_5O_{12}$ (LTO) has been extensively investigated as one of the leading candidates because of its almost zero volume change (0.25%) during Li insertion/extraction [10], which leads to high safety by preventing the formation of solid-electrolyte interface (SEI). However, its low electrical conductivity (10^{-13} S cm^{-1}), low lithium diffusion coefficient (10^{-9} to 10^{-13} cm^2 S^{-1}), low capacity (175 mA h g^{-1}), and relatively high voltage plateau (~1.55 V) limit its applications [11]. As a result, insufficient lithiation/delithiation at high rates results in low full cell voltage. Reducing the size of LTO to nanoscale (*e.g.* nanowire [12], nanotube [13]), one of effective methods to enhance lithium diffusion, significantly favors the improvement of rate capability and cyclic stability. Moreover, using woven/nonwoven carbon cloth (CC) as the supporting material for LTO nanostructures improves the performance through enhancing the conductivity [14], serving as electron collector, and avoiding the use of binders, which are electrical insulator without electrochemical capacity [15]. More importantly, the CC substrate renders

* Corresponding author.
E-mail address: baichengweng@hotmail.com (B. Weng).

http://dx.doi.org/10.1016/j.jpowsour.2017.04.034
0378-7753/

the application of LTO in flexible devices, such as rollup display, smart card, and wearable devices, due to its good flexibility, conductivity, stability and excellent mechanical properties [16]. However, the capacity of CC supported LTO nanostructures should be further enhanced. Since carbon is inactive to lithium at the potential above 1 V (vs. Li/Li^+), it will not contribute to the energy density of the electrode [9].

Recently, $NiCo_2O_4$ (NCO) has drawn many attentions as an alternative material of Co_2O_3 for LIBs, owning to its high electrical conductivity and theoretical specific capacity (884 mA h g^{-1}) and low working potential (0.3–2.3 V) [17]. It, however, experiences great volume change during lithium insertion/extraction [18]. Herein, given that the characteristics of these two electrochemically active materials of LTO and NCO, we complementarily integrated LTO and NCO together, and thus rationally designed and fabricated the hierarchical CC supported LTO@NCO branched nanowire (NW) arrays (CC/LTO@NCO), which feature the homogenous growth of NCO NW branches as the shell on the surface of CC supported LTO NWs (CC/LTO) as the core. The almost zero volume change nature of LTO can prevent NWs from failing caused by volume change, thus ensuring the stability of the composite. More strikingly, the novel CC/LTO@NCO composite with high flexibility reveals significantly improved electrochemical properties as an anode for LIBs compared with CC/LTO. Specifically, the binder-free composite exhibits a superior specific capacity of 298 mA h g^{-1} at 1 C, a remarkable high-rate performance of 203 mA h g^{-1} at 20 C as well as excellent cyclic stability with capacity retention of 97% for 1200 cycles at 1 C.

2. Experimental

2.1. Material synthesis

Carbon cloth supported TiO_2 NWs (CC/TiO_2) were firstly prepared. Typically, 0.3 mL $Ti(OBu)_4$ was slowly dropped into a mixture solution of 13 mL HCl and 15 mL H_2O, followed by vigorously stirring for 30 min. The solution and CC were then transferred into a hydrothermal autoclave at 180 °C for 12 h. After the autoclave was cooled to room temperature by quenching with water, the sample was ultrasonically cleaned for 3 min in a 2:1 (v/v) mixture of isopropyl alcohol and H_2O, and dried under vacuum. Subsequently, stoichiometric amount of LiOH, which was dissolved in methanol, was dropped on the CC/TiO_2 sample and dried under nitrogen flow. The obtained sample was calcinated at 750 °C for 12 h at a ramping speed of 2 °C min^{-1} to obtain CC/LTO NWs. Ni and Co seeds were loaded on the surface of the as-prepared CC/LTO sample through dipping in 5 mM $Ni(OAc)_2$ and $Co(NO_3)_2$ acetone solution for 4 times followed by being calcinated at 350 °C for 30 min on hot plate. NCO NWs were grown on the surface of LTO NWs through a hydrothermal reaction in a solution containing 40 mM $Ni(NO_3)_2$, 80 mM $Co(NO_3)_2$ and 480 mM urea at 80 °C for 6 h. After the autoclave was cooled to room temperature naturally, the sample was rinsed with water and dried under vacuum. The as-obtained materials were annealed at 300 °C for 2 h to get CC/LTO@NCO NWs.

2.2. Material characterization

The morphology of the samples was observed using a scanning electron microscope (SEM, Sigma VP, Carl Zeiss, Germany). The high-resolution transmission electron microscopy (HRTEM) images were taken on a JEOL-2010 TEM at an acceleration voltage of 200 kV. Powder X-ray diffraction patterns (XRD) were recorded on Bruker D8 Advance ECO diffractometer equipped with graphite monochromatized high-intensity Cu/K*a* radiation ($\lambda = 1.54178$ Å). X-ray photoelectron spectra (XPS) were collected on a physical electronics PHI5400 using Mg/K*a* radiation as the X-ray source. The specific surface area was calculated from N_2 adsorption–desorption isotherms measured at 77 K on an ASAP-2010 surface area analyzer. The specific surface area was calculated from the adsorption curve according to the Barrett-Joyner- Halenda (BJH) method.

2.3. Electrochemical measurements

The cells (CR2032) were assembled in a glovebox (Mbraun, LabMaster 100, Germany) under an argon atmosphere by using the as-synthesized hierarchical NW arrays as the anode. For the flexible battery, each electrode was cut into a rectangle of 3 × 1 cm with a narrow strip on edge to connect with wires. The electrodes and separator were immersed in electrolyte for 12 h before the battery was assembled and sealed by flexible plastic bag using edge-bonding machine. All the electrochemical measurements were performed using an Autolab PGSTAT302N. The counter and reference electrodes were lithium chips, and the electrolyte solution was 1M $LiPF_6$, in which the solvent mixture was ethylene carbonate (EC)/dimethyl carbonate (DMC)/ethyl methyl carbonates (EMC) (1:1:1 in volume). The cells were charged and discharged over a voltage range of 0.05–3 V vs. Li^+/Li at room temperature. Cyclic voltammetry was performed in the range of 0.05–3.0 V vs. Li^+/Li at a scan rate of 0.5 mV s^{-1}. Constant-current charge/discharge tests were carried out at different current densities in the same voltage range. The interfacial resistance was investigated using EIS over the frequency range of 1 MHz to 1 Hz under AC stimulus with 10 mV of amplitude and no applied voltage bias. Before the EIS measurements, the electrodes were cycled for three times, then charged to 3.0 V and kept until the open-circuit voltage was stabilized.

3. Results and discussion

Fig. 1 shows fabricating schematic of the hierarchical carbon cloth supported $Li_4Ti_5O_{12}/NiCo_2O_4$ branched nanowire arrays (CC/LTO@NCO). First, TiO_2 NWs were grown on carbon cloth (CC) via a facile hydrothermal method[17] and then lithiated to $Li_4Ti_5O_{12}$ (LTO) through a solid-state reaction [10]. $NiCo_2O_4$ (NCO) NWs, subsequently, were homogeneously and orthogonally grown on the surface of LTO NWs during another seed-assistant hydrothermal process, resulting in the formation of CC/LTO@NCO branched NW arrays.

Scanning electron microscopy (SEM, Fig. 2a–c) reveals that the surface of carbon fibers in the CC is uniformly covered by TiO_2 NWs with an average diameter of 70 nm and a length of 1.2 μm, forming an initial hierarchical structure. After the following lithiation process (Fig. 2d), the NW arrays have a rougher surface and larger diameter of 90 nm due to the volume expansion caused by the density difference between LTO and TiO_2 [10]. The perpendicular growth of NCO NWs onto the surface of LTO NWs leads to the generation of a secondary hierarchical architecture with branched NW arrays (Fig. 2e and f). The needle-like NCO NWs exhibit a diameter of 20–30 nm and a length of 400–500 nm. High-resolution transmission electron microscopy (HRTEM) images show that the observed 0.486 nm lattice spacing corresponds to the (111) atomic plane of cubic LTO (Fig. 2g), while the 0.287 nm lattice spacing is consistent with the (220) atomic plane of orthorhombic NCO (Fig. 2h). The crystal structure was further verified by X-ray diffraction (XRD) measurements (Fig. 2i). The pattern of TiO_2 NWs coated CC sample (CC/TiO_2) is in good agreement with rutile-type TiO_2 (space group $P4_2/mnm$, no. 136) and graphitic carbon (space group $P6_3mc$, no. 186), which confirms the SEM observation that rutile TiO_2 NWs are successfully grown on the CC after the first hydrothermal reaction. Further lithiation through solid-state reaction leads to complete conversion of rutile TiO_2 to spinel-type LTO

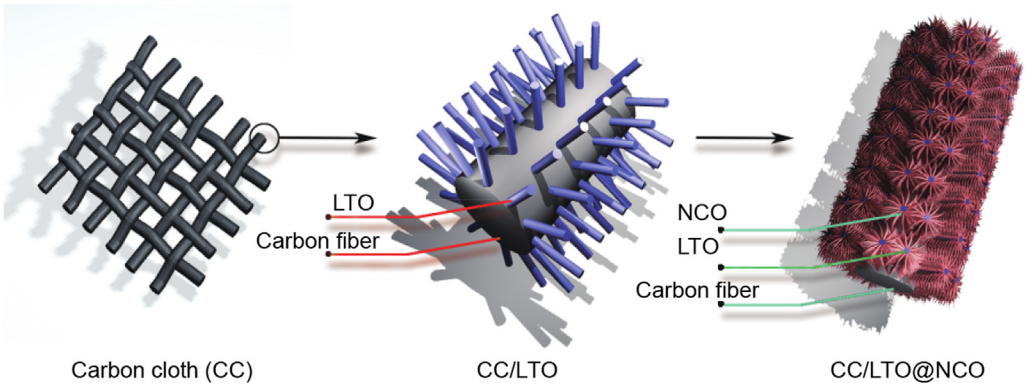

Fig. 1. Fabricating route of hierarchical CC/LTO@NCO branched NWs.

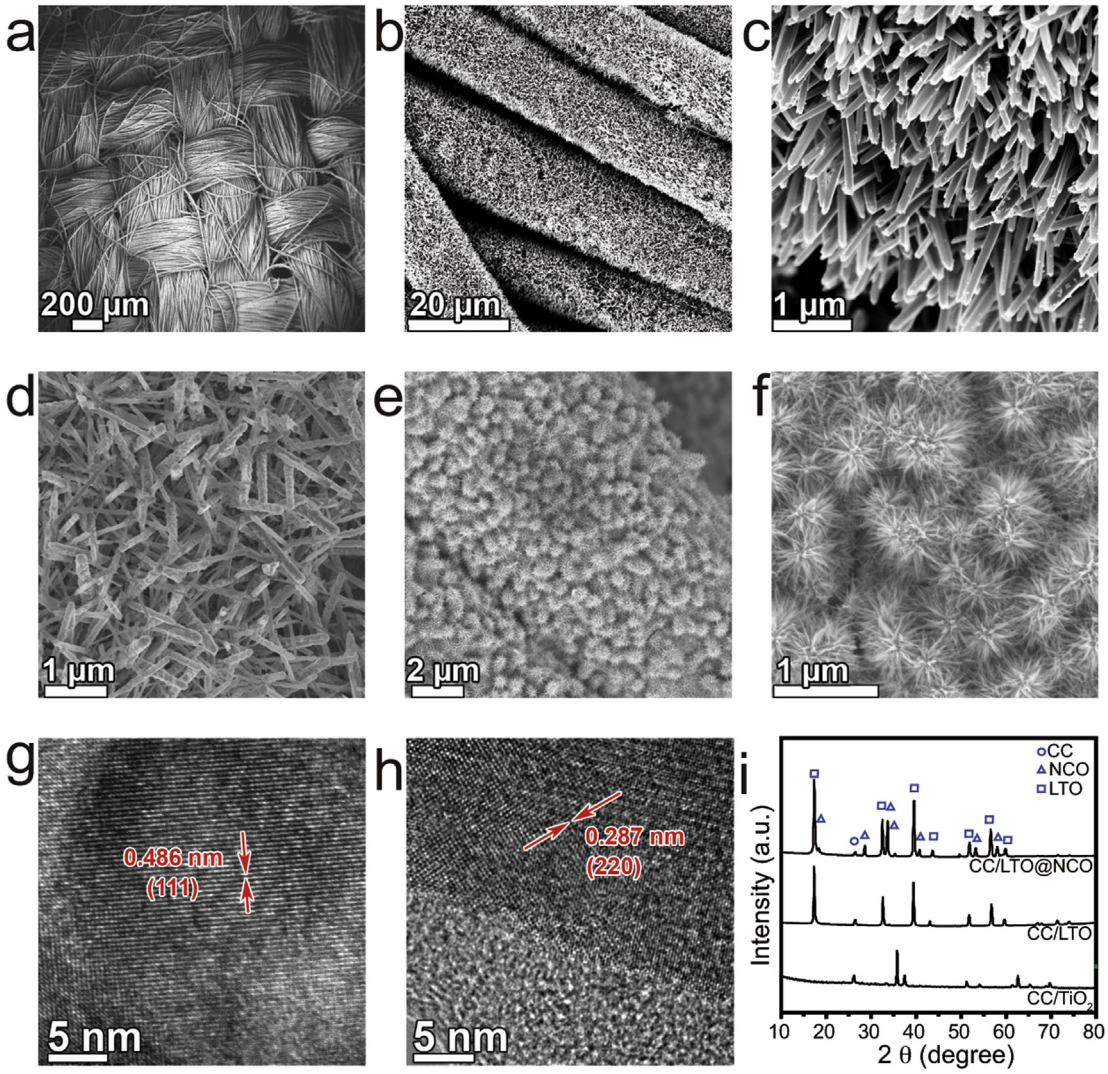

Fig. 2. Morphology and structural characterizations of CC supported TiO_2 NWs, LTO NWs, and LTO@NCO NWs. (a)–(c) SEM images of CC/TiO_2 NWs. (d) SEM image of CC/LTO NWs. (e)–(f) SEM images of CC/LTO@NCO NWs. (g) HRTEM image of LTO NWs. (h) HRTEM image of NCO NWs. (i) XRD patterns of CC supported TiO_2 NWs, LTO NWs, and LTO@NCO NWs.

(space group $Fd\bar{3}m$, no. 227). Compared with the CC/LTO, XRD pattern of the CC/LTO@NCO composite exhibits an extra phase, which assigned to spinel-type NCO (space group $Fd\bar{3}m$, no. 227, JCPDS card no. 20–0781). Besides, the CC/LTO@NCO composite was subjected to X-ray photoelectron spectroscopy (XPS) study to further identify the chemical composition and states. Fig. 3a–d show high-resolution XPS spectra of Ti 2p, Ni 2p, Co 2p, and O 1s core level peaks, respectively. The peaks in the range from 856.5 to 872.8 eV (Fig. 3a) can be ascribed to Ni^{2+} [20]. The peaks at 780.2 and 797.8 eV correspond to Co^{3+} in NCO (Fig. 3b) [21]. The peaks at

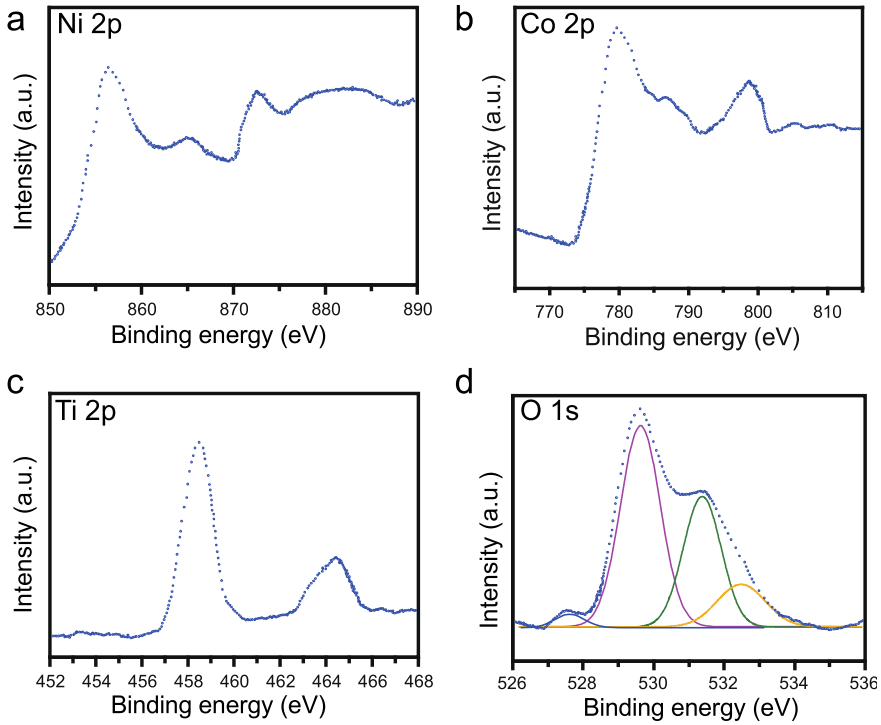

Fig. 3. XPS spectra of (a) Ni 2p, (b) Co 2p, (c) Ti 2p, and (d) O1s in the CC/LTO@NCO composite.

458.6 and 464.3 eV (Fig. 3c) are assigned to Ti $2p_{3/2}$ and Ti $2p_{1/2}$, respectively, with a typical Ti 2p spin-orbit splitting of 5.7 eV, which is the characteristic of Ti^{4+} in LTO [22]. The peaks of O 1s (Fig. 3d) are contributed by lattice oxygen of Ni—O, Ti—O and Co—O bonds at 529.4, 531.2 and 532.8 eV, respectively, and the surface adsorbed oxygen at 527.6 eV. Thus, the XPS result further suggests the successfully continuous growth of LTO and NCO on the CC. The content of LTO and NCO is determined by XPS to be about 25 wt% and 5 wt%. The characterizations well exhibit that the CC/LTO@NCO composite presents a hierarchical branched NW structure, featuring highly crystallized NCO orthogonally grown on LTO NWs, which vertically coat on the surface of CC. The formation of NW branches enhances the surface area and hence could shorten the lithium immigration length as well as expose more active site, facilitating lithium immigration during lithiation/delithiation process and therefore favoring the improvement of electrochemical activities.

Next, the electrochemical performance of the CC/LTO@NCO composite was evaluated as the anode for LIBs. Fig. 4a shows cyclic voltammogram (CV) curves of the CC/LTO@NCO composite at a scan rate of 0.5 mV s^{-1} with a cut-off voltage of 0.05–3 V. The current peak at 1.30 V for the first cycle, which shifts to 1.41 V for the second and third cycles, corresponds to lithiation of LTO; while the peaks at 1.62 V for all three cycles are ascribed to delithiation of LTO, in good accordance with the previous report [10]. Cathodic current peaks centered at 0.58 V for the first cycle and at 0.75 V for the second and third cycles can be attributed to the reduction of Ni^{2+} and Co^{3+} to Ni and Co, respectively. The anodic current peaks around 2.1 V are assigned to the oxidation of Co to Co^{3+}. The shift of peak position for the second and third cycles can be attributed to the formation of solid-electrolyte interface (SEI) [19]. More strikingly, the CV curves for the second and third cycles exhibit good reproducibility with almost the same peak current and integrated area of the cathodic/anodic peak, suggesting high reversibility of lithium storage of the CC/LTO@NCO composite. As shown in Fig. 4b, the charge/discharge curves of CC/LTO at different current rates from 1 to 20 C display slow voltage plateaus around 1.5 V, reflecting Femi level changes between LTO and $Li_7Ti_5O_{12}$ phases during lithiation and delithation processes [10]; while after growth of the dense and uniform NCO NW branches on the surface, the obvious plateaus are no more observed. Notably, the CC/LTO delivers a specific discharge capacity of 172 mA h g^{-1} at the initial low rate of 1 C, which is very close to the theoretical capacity of LTO (175 mA h g^{-1}), whereas the CC/LTO@NCO composites exhibit a much higher capacity of 298 mA h g^{-1} owing to capacity contribution from branched NCO NWs with high electrical conductivity and theoretical specific capacity (884 mA h g^{-1}). The enhanced capacity reveals the improvement of Li electroactivity by the formation of the branched NCO NWs coating.

High mass loading of active materials and high volumetric capacity are still one of challenges for nanostructured materials, due to difficulties to achieve robust electronic and ionic connections between neighboring nanoparticles [23]. The developed anode has a mass loading of 6.29 mg cm^{-2}, which is higher than that of the reported CC supported LTO or NCO nanostructures (usually 1.0–5.1 mg cm^{-2}, depending on the structure) [24]. The unique structure of hierarchical CC supported LTO@NCO branched NWs enhances the loading of active materials, and thus benefits the improvement of gravimetric and volumetric capacity. CC/LTO@NCO composites can deliver areal capacity of 1.87 mA h cm^{-2}, which is higher than that of NCO NWs grown on CC [24]. And the corresponding volumetric capacity is determined to be 51.94 mA h cm^{-3}, based on the CC thickness of 360 μm, given that the commercialized CC with an average diameter of 10 μm is used in this study.

The rate performance of the CC/LTO@NCO composite at various current densities ranging from 1 C to 20 C was also investigated, compared to that of the CC/LTO (Fig. 4b). For each current rate, 20 cycles were conducted. The CC/LTO@NCO composite exhibits excellent rate performance. The specific discharge capacity decreases slightly and slowly from 298 mA h g^{-1} at the rate of 1 C–262 mA h g^{-1} at 3 C, 250 mA h g^{-1} at 5 C, and 235 mA h g^{-1} at 10 C. Even at a very high rate of 20 C, the specific discharge capacity

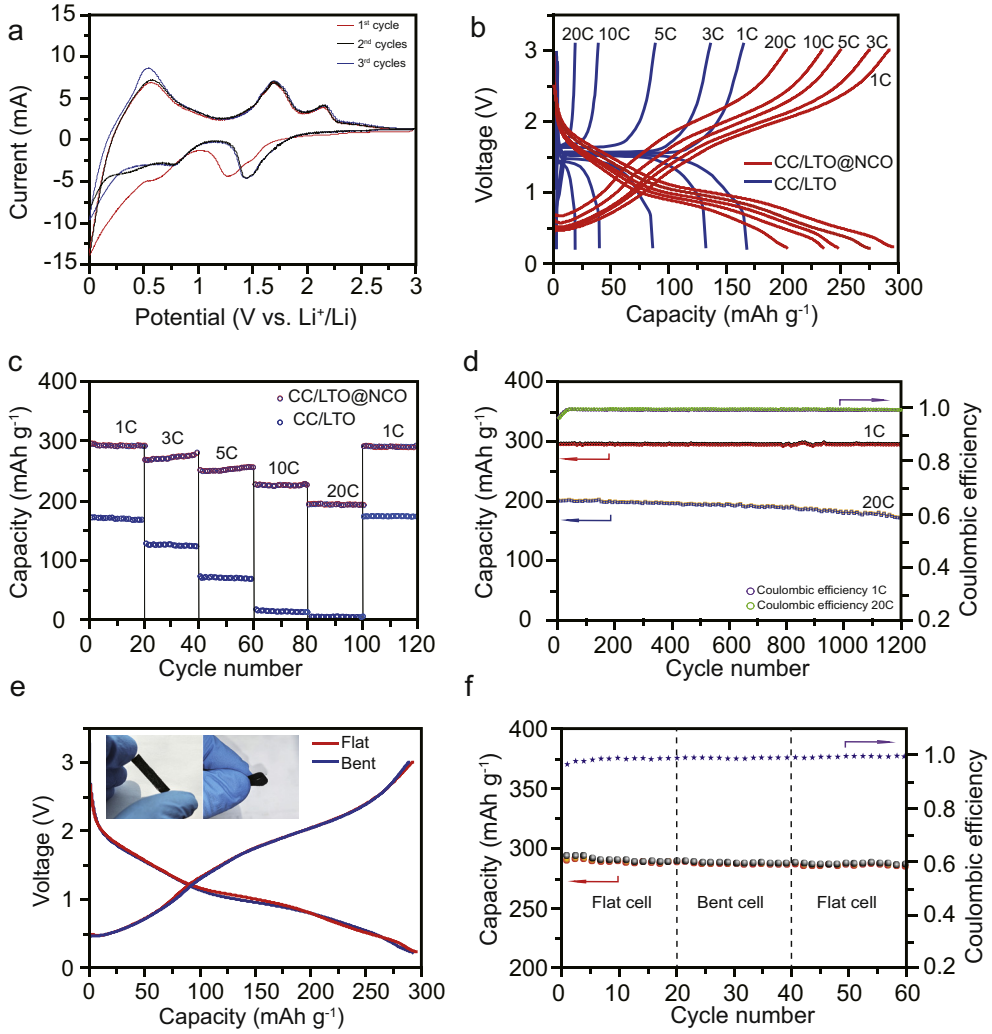

Fig. 4. Electrochemical performance of the CC/LTO@NCO electrode. (a) CV curves of the CC/LTO@NCO composite for the first, second, and third cycles at a scan rate of 0.5 mV s^{-1}. (b) Charge/discharge curves of CC/LTO and CC/LTO@NCO between 0.05 and 3 V at different current rates. (c) Rate performance of CC/LTO and CC/LTO@NCO at different current rates. (d) Cyclic stability performance at the rates of 1 C and 20 C as well as the corresponding Coulombic efficiency at the rate of 1 C. (e) Comparison of charging/discharging curves of the flat and bent batteries after 20 times bending. Inserted image in (e) is photograph of flexible CC/LTO@NCO electrode material. (f) Cyclic performance of the flat and bent batteries.

still reaches to 203 mA h g^{-1}, which is even much greater than that of the CC/LTO at the low rate of 1 C (172 mA h g^{-1}). The CC/LTO, however, shows remarkably decreased capacity from 1 C (172 mA h g^{-1}) to 20 C (14 mA h g^{-1}). More importantly, the CC/LTO@NCO composite displays good capacity retention at various rates. When the rate is reduced back to 1 C after more than 100 cycles, a stable original discharge capacity (~298 mA h g^{-1}) is recovered, demonstrating excellent electrochemical reversibility. Furthermore, the cyclic performance of the CC/LTO@NCO composites was evaluated at the charge/discharge rates of 1 C and 20 C (Fig. 4d). The CC/LTO@NCO composites display outstanding capacity retention with slight capacity declination of ~3% at 1 C and 14% at 20 C over 1200 charge/discharge cycles, suggesting the excellent cyclic performance. And the Coulombic efficiency keeps at almost 100%. This result demonstrates that the CC/LTO@NCO is very stable, and the electrochemical Li^+ insertion/extraction process is quite reversible. The excellent rate performance and cyclic stability of the CC/LTO@NCO composite in the voltage range from 0.05 to 3 V manifest good application potentials for high-power outputs at low working voltage. It is worth noting that the CC/LTO@NCO electrode exhibits good flexibility with bending more than 180 °C (inserted image in Fig. 4e). After 20 bends, the battery shows negligible change in capacity and overpotential, compared with that of the original flat battery (Fig. 3e). Furthermore, the flexible battery exhibits an excellent cyclic stability even after bending. The capacity retention is ~98% after the first 20 cycles without bending and ~96% after another 20 cycles with bending (Fig. 3f). The observation well demonstrates the excellent stability and capacity retention of the CC/LTO@NCO anode under bending. The outstanding electrochemical properties may be attributed to the synergetic effect of outer NCO and core LTO. NCO has high capacity and electrical conductivity but suffers large volume change during lithiation/delithiation, which in turn reduces the cyclability; whereas LTO possesses the almost zero volume change during charge/discharge process, which enables LTO the ideal core material, although it has a low capacity. Therefore, in this study, LTO as core material and NCO as shell material are continuously and hierarchically grown on the surface of the flexible CC, which could complementarily take advantage of the stability of LTO and high capacity of NCO as well as the flexibility of CC.

In order to verify the effect of NCO NW branches covering on the surface of CC/LTO, Brunauer-Emmett-Teller (BET) measurements

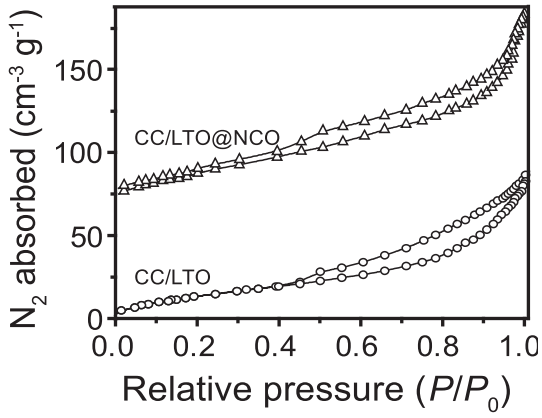

Fig. 5. N_2 adsorption–desorption isotherms measured at 77 K of CC/LTO and CC/LTO@NCO, respectively.

were firstly conducted (Fig. 5). The CC/LTO@NCO composites exhibit a much higher specific surface area of 174.5 $m^2 g^{-1}$ than that (98.2 $m^2 g^{-1}$) of CC/LTO. Therefore, the CC/LTO@NCO electrode can deliver more contact with Li^+ ion in the electrolyte, benefiting the improved lithium diffusion and intercalation. Next, the electrochemical impedance spectroscopy (EIS) was carried out to evaluate charge transfer in the anode before and after 120 charge/discharge cycles, compared with that of CC/LTO (Fig. 6), and the fitting data are shown in Table 1. The semicircular arc diameter in the curves is related to charge transfer resistance (R_{ct}) [25,26]. The semicircular arc diameter of the CC/LTO@NCO composite decreases compared with that of the CC/LTO, indicating that the CC/LTO@NCO electrode has a lower charge transfer resistance. Thus the NCO NWs coating results in faster charge transfer and improved lithium diffusion, which may arise from the large surface area and high conductivity after coating. Therefore, the unique structure of hierarchical CC supported LTO@NCO branched NWs composite also benefits the superior electrochemical properties. The curve after cycling is composed of two partially overlapped semicircles in the high-to-medium frequency range and a low frequency sloping line, which is an evidence of the SEI formation. Such an EIS pattern can be fitted by an equivalent circuit shown in the inset, where R_s is the bulk resistance of the cell, reflecting the electric conductivity of electrolyte, separator and electrodes; R_{sei} and C_{sei} are the resistance and capacitance of SEI, corresponding to the first semicircle at high frequency [27]. After 120 charge/discharge cycles, the shape of the EIS curve shows a small change, indicating that the SEI formation does not increase the ionic and electronic resistance and inhibit the charge transfer process in the significant way. Then small R_s and R_{ct} differences before and after charge/discharge cycles suggest good electrons transfer between the electrode and current collector as well as charge transfer. The low volume-change of the core material LTO during charge/discharge prevents the formation of thick SEI, and thus benefits the charge transfer.

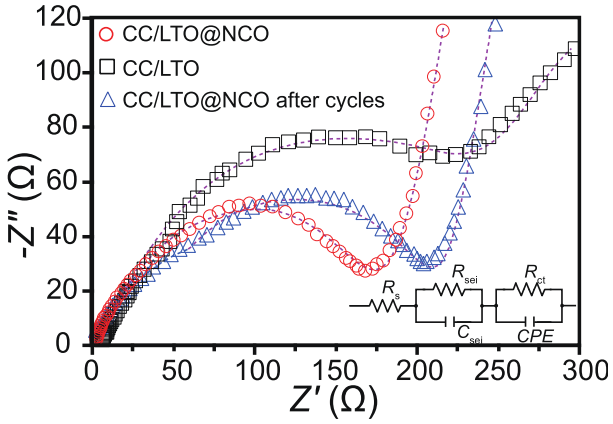

Fig. 6. EIS plots of CC/LTO and CC/LTO@NCO before and after 120 charge/discharges cycles, respectively. Inserted circuit model: R_s, resistance of solution; R_{ct}, charge transfer resistance; *CPE*, constant phase element; R_{sei}, the resistance of SEI and C_{sei}, the capacitance of SEI.

Table 1
Equivalent circuit parameters obtained from EIS measurements.

Sample	R_s (Ω)	R_{ct} (Ω)
CC/LTO	9.1	315.9
CC/LTO@NCO	3.7	184.3
CC/LTO@NCO after cycles	5.0	190.2

4. Conclusions

We have successfully developed a novel, binder-free CC/LTO@NCO composite by first coating LTO NWs on the surface of carbon cloth, followed by the orthogonal growth of NCO NW branches on the CC/LTO NWs. Benefiting from the unique hierarchical structure and the synergetic effect of CC/LTO and NCO, the flexible composite exhibits remarkable specific capacity, high rate capability, and excellent long-term cyclic performance with 97% capacity retention over 1200 cycles at 1 C when used as anode for lithium-ion batteries. This novel composite electrode holds the promising use in flexible LIBs.

Acknowledgement

This work is supported by National Science Foundation of Jiangsu Province, China (Grant No. BK20150428).

References

[1] G. Xu, Y. Tian, X. Wei, L. Yang, P.K. Chu, J. Power Source 337 (2017) 180–188.
[2] Y. Wang, G.Z. Cao, Adv. Mater 20 (2008) 2251–2269.
[3] B. Weng, W. Wei, Yiliguma, H. Wu, A.M. Alenizi, G. Zheng, J. Mater. Chem. A 4 (2016) 15353–15360.
[4] B. Weng, F. Xu, C. Wang, W. Meng, C.R. Grice, Y. Yan, Energy Environ. Sci. 10 (2017) 121–128.
[5] H. Ge, L. Chen, W. Yuan, Y. Zhang, Q. Fan, H. Osgood, D. Matera, X.M. Song, G. Wu, J. Power Source 297 (2015) 436–441.
[6] L. Croguennec, M.R. Palacin, J. Am. Chem. Soc. 137 (2015) 3140–3156.
[7] Y. Wang, J. Zeng, J. Li, X. Cui, A.M. Al-Enizi, L. Zhang, G. Zheng, J. Mater. Chem. A 3 (2015) 16382–16392.
[8] N. Li, Z. Chen, W. Ren, F. Li, H.M. Cheng, PNAS 109 (2012) 17360–17365.
[9] Z.L. Wang, D. Xu, H.G. Wang, Z. Wu, X.B. Zhang, ACS Nano 7 (2013) 2422–2430.
[10] L. Yu, H.B. Wu, X.W. Lou, Adv. Mater. 25 (2013) 2296–2300.
[11] L. Shen, C. Yuan, H. Luo, Zhang, X.K. Xu, Y. Xia, J. Mater. Chem. 20 (2010) 6998–7004.
[12] Y.Q. Wang, L. Gu, Y. Guo, H. Li, X.Q. He, S. Tsukimoto, Y. Ikuhara, L.J. Wan, J. Am. Chem. Soc. 134 (2012) 7874–7879.
[13] L. Sun, W. Kong, H. Wu, Y. Wu, D. Wang, F. Zhao, K. Jiang, Q. Li, J. Wang, S. Fan, Nanoscale 8 (2016) 617–625.
[14] X. Lu, L. Gu, Y.S. Hu, H.C. Chiu, H. Li, G.P. Demopoulos, L. Chen, J. Am. Chem. Soc. 137 (2015) 1581–1586.
[15] Y. Shi, L. Wen, F. Li, H.M. Cheng, J. Power Source 196 (2011) 8610–8617.
[16] K. Qiu, Y. Lu, D. Zhang, J. Cheng, H. Yan, J. Xu, X. Liu, J.K. Kim, Y. Luo, Nano Energy 11 (2015) 687–696.
[17] Y. Huang, Y.E. Miao, H. Lu, T. Liu, Chem. Eur. J. 21 (2015) 10100–10108.
[18] L. Shen, L. Yu, X.Y. Yu, X.G. Zhang, X.W. Lou, Angew. Chem. Int. Ed. 53 (2014) 1–6.
[19] M.G. Verde, L. Baggetto, N. Balke, G.M. Veith, J.K. Seo, Z. Wang, Y. Meng, ACS Nano 10 (2016) 4312–4321.
[20] W. Xiong, X. Hu, X. Wu, Y. Zeng, B. Wang, G. He, Z. Zhu, J. Mater. Chem. A 3 (2015) 17209–17216.
[21] S. Wang, J. Pu, Y. Tong, Y. Cheng, Y. Gao, Z. Wang, J. Mater. Chem. A 2 (2014) 5434–5440.

[22] G. Xu, L. Yang, X. Wei, J. Ding, J. Zhong, P.K. Chu, Adv. Funct. Mater. 26 (2016) 3349–3358.
[23] Z. Lu, N. Liu, H.W. Lee, J. Zhao, W. Li, Y. Li, Y. Cui, ACS Nano 9 (2015) 2540–2547.
[24] L. Shen, Q. Chen, H. Li, X. Zhang, Adv. Funct. Mater. 24 (2014) 2630–2637.
[25] L. Qian, L. Gu, L. Yang, H. Yuan, D. Xiao, Nanoscale 3 (2015) 7388–7396.
[26] C. Shang, S. Dong, S. Wang, D. Xiao, P. Han, X. Wang, L. Gu, G. Cui, ACS Nano 7 (2013) 5430–5436.
[27] C. Wang, A.J. Appleby, F.E. Little, Electrochim. Acta 46 (2001) 1793–1813.